

# Fluxoid dynamics in superconducting thin film rings

J. R. Kirtley and C. C. Tsuei

IBM T.J. Watson Research Center, P.O. Box 218, Yorktown Heights, NY 10598

V. G. Kogan and J. R. Clem

Ames Laboratory and Department of Physics and Astronomy, Iowa State University, Ames, IA 50011

H. Ray and Z. Z. Li

Laboratoire de Physique des Solides, Université Paris-Sud, 91405 Orsay, France

(Dated: May 16, 2019)

We have measured the dynamics of individual magnetic vortices entering and leaving photolithographically patterned thin film rings of the underdoped high-temperature superconductor  $B_{1-x}Sr_xCaCu_2O_{8+\delta}$ , using a variable sample temperature scanning SQUID microscope. These results can be qualitatively described using a model in which the vortex number changes by thermally activated nucleation of a Pearl vortex, and transport of the Pearl vortex across the ring wall.

PACS numbers: 47.32.Cc, 74.25.Qt, 85.25.Cp

## I. INTRODUCTION

Although vortex quantization in superconductors was first demonstrated experimentally over 40 years ago,<sup>1,2</sup> there has recently been a resurgence of interest in vortex dynamics in a ring geometry. For example, it has been proposed that the interacting dipole moments in an array of superconducting rings can provide a model experimental system for studying magnetism in Ising antiferromagnets.<sup>3,4,5,6,7</sup> This possibility has become particularly attractive with the development of  $\phi$ -rings: superconducting rings with an intrinsic quantum mechanical phase change of  $2\pi$  upon circling the ring, in the absence of supercurrents or externally applied fields. Such phase changes can be produced either by the momentum dependence of an unconventional superconducting order parameter,<sup>8,9,10,11,12</sup> or by magnetic interactions in the tunneling region of a Josephson weak link in the ring.<sup>13,14,15</sup>  $\phi$ -rings are an ideal model system for the Ising antiferromagnet, since they have a degenerate, time-reversed ground state in the absence of an externally applied magnetic field. Recent progress<sup>16,17</sup> has made it possible to reliably make very large closely packed arrays of  $\phi$ -rings, which show strong antiferromagnetic correlations in their "spin" orientations upon cooling in zero magnetic field.<sup>18</sup> Superconducting ring experiments have also been proposed<sup>19</sup> and performed<sup>20,21</sup> to test for the presence of "visons", vortex-like topological excitations which may result from electron fractionalization in the high- $T_c$  cuprate superconductors. In addition, superconducting rings can provide a model system for the early evolution of the universe, through the study of quenched fluctuations in superconducting rings.<sup>22,23,24,25,26,27,28</sup> Each of these studies depend critically on an understanding of the vortex dynamics during the cooldown process. Finally, there has been a resurgence of interest lately in macroscopic quantum coherence effects in superconducting rings, in conjunction with

applications to quantum computation.<sup>29,30,31</sup> In these experiments noise due to thermally activated motion of vortices must be considered, at least at elevated temperatures. Therefore the study of vortex dynamics in rings is one of much current topical interest.

Thermally activated vortex dynamics in superconductors have been studied extensively,<sup>32</sup> including in ring geometries.<sup>33</sup> Magnetic noise in high temperature cuprate superconductors has been shown to arise from thermally activated hopping of vortices between pinning sites.<sup>34</sup> Fluxoid dynamics have been studied in superconducting rings interrupted by Josephson weak links,<sup>35</sup> and in mesoscopic rings, with the coherence length comparable to the ring dimensions.<sup>36</sup> However, the system we have chosen to study, relatively large rings with long magnetic penetration depths (because they are strongly underdoped), is in many respects a particularly simple one. First, our rings have no intentional Josephson weak links. Many quantitative details specific to phenomena related to vortex quantization can be treated within the London approach, which is not bound by the rigid temperature restriction of the Ginzburg-Landau theory. The smallness of the ring with respect to the Pearl length<sup>37</sup>  $\lambda_P = 2\lambda/d$  (in the thin film limit, the London penetration depth  $\lambda$ , the film thickness) simplifies considerably the problem of a ring in an applied magnetic field. Studies of the transitions between quantum states in thin film rings are relevant for understanding the dynamics of multiply connected mesoscopic superconducting devices in general and of the telegraph noise in these devices in particular.

## II. EXPERIMENTAL RESULTS

Our measurements were made on 300 nm thick films of the high-temperature superconductor  $B_{1-x}Sr_xCaCu_2O_{8+\delta}$  (BSCCO), epitaxially grown on (100) SrTiO<sub>3</sub> substrates using magnetron sputtering. The oxygen concentration

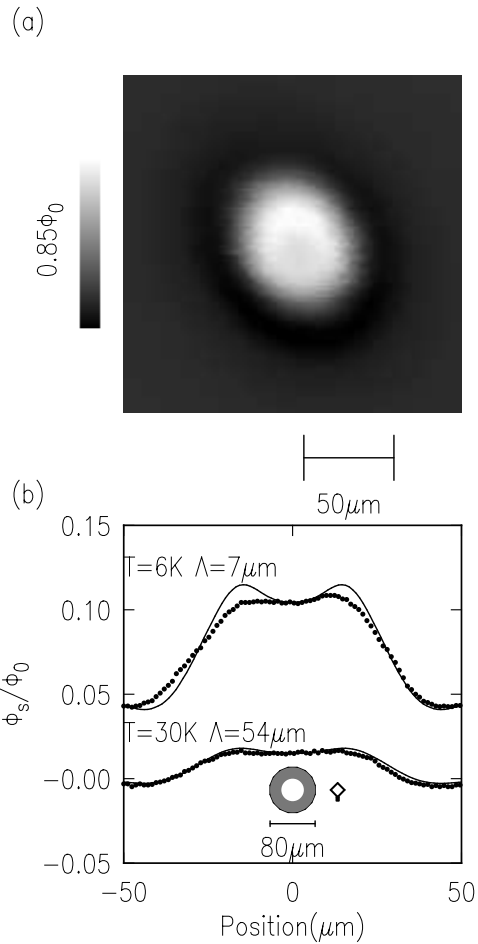


FIG. 1: (a) Scanning SQUID microscope image of an 80  $\mu\text{m}$  diameter ring cooled in a magnetic induction of 6.9 mG, resulting in a vortex number of  $N = 10$ , and imaged in zero field at  $T = 6\text{ K}$ . (b) Cross-sections through the center of the ring in (a), cooled in an induction of 0.7 mG, resulting in a vortex number of  $N = 1$ , and imaged in zero field at temperatures of 6 K and 30 K (dots), and modelling as described in the text (line). The data and fit for  $T = 6\text{ K}$  have been offset vertically by  $0.05 \phi_0$  for clarity. The insets at the bottom of (b) show schematics of the ring and SQUID pickup loop geometries.  $\phi_s$  is the flux through the SQUID pickup loop.

in these films was varied by annealing in oxygen or argon at 400–450  $^\circ\text{C}$ . The films were photolithographically patterned into circular rings using ion etching. The rings had outside diameters of 40, 60, and 80  $\mu\text{m}$ , with inside diameters half the outside diameters. The film for the current measurements had a broad resistive transition (90% of the extrapolated normal state resistance at  $T = 79\text{ K}$ , 10% at  $T = 46\text{ K}$ ) with a zero-resistance  $T_c$  of 36 K before patterning. Such broad resistive transitions are characteristic of both single crystals<sup>38</sup> and thin films<sup>39</sup> of BSCCO, and may be indicative of oxygen inhomogeneity. In this paper we will treat the rings as homogeneous and cylindrically symmetric. This view is supported by two facts: 1) the SQUID images are hom-

ogeneous, at least within the spatial resolution set by the 17.8  $\mu\text{m}$  pickup loop size, at all temperatures (see e.g. Fig. 1); and 2) the Pearl penetration depth is quite long, of order 100  $\mu\text{m}$ , at the temperatures of interest. This long penetration depth might be expected to average out spatial inhomogeneities. Nevertheless, it is possible that the vortex transitions in our samples are dominated by paths with relatively low barrier heights.<sup>33</sup> It is therefore remarkable that the simple model described in this paper qualitatively describes our results in the presence of this inhomogeneity. The critical temperatures of the rings were slightly lower after patterning than the blanket coverage film, presumably due to additional oxygen removal in the ion etching step. The critical temperature of the individual ring being measured was determined by SQUID inductive measurements, as described below. The rings were magnetically imaged using a variable sample temperature scanning Superconducting Quantum Interference Device (SQUID) microscope,<sup>40</sup> which scans a sample relative to a SQUID with a small, well shielded, integrated pickup loop (a square loop 17.8  $\mu\text{m}$  on a side for these measurements), the sample temperature being varied while the low- $T_c$  SQUID remains superconducting.

Figure 1 (a) shows a scanning SQUID microscope image of an 80  $\mu\text{m}$  outside diameter ring, cooled in an induction of 6.9 mG, which results in a vortex number  $N = 10$  in the ring, and imaged in zero field at low temperature. For consistency, all of the measurements presented in this paper were made on this ring. Measurements on a number of rings of all three sizes were also performed, with quite comparable results. The dots in Figure 1 (b) are cross-sections through the center of the 80  $\mu\text{m}$  ring with a ring vortex number of  $N = 1$  in zero field at two temperatures. The solid lines are fits to the SSM images, taking into account the detailed current distributions in the rings. Such fits are used in this paper to determine the temperature-dependent Pearl penetration length  $\lambda$ , which is an important parameter in modelling the vortex dynamics.

Fig. 2 shows the results of a number of such measurements as a function of temperature on this ring. The solid circles in Fig. 2a are the difference  $\phi_s$  between the SQUID signal with the pickup loop centered over the ring and that with the pickup loop far from the ring, with the ring in the  $N = 1$  vortex state. Such measurements cannot be made closer than about 1K from  $T_c$  because the ring switches to the  $N = 0$  state. The solid diamonds are measurements  $\phi_s$  with a small applied induction  $B_a = 0.2\text{ mG}$  with the ring in the  $N = 0$  state. The squares are the change in the flux through the SQUID when the ring spontaneously changes vortex number in the telegraph noise described below. The dashed line is a linear extrapolation of the  $\phi_s$  (circles and squares) data; the zero crossing of this line provides an estimate of the critical temperature  $T_c$  for this ring,  $T_c = 32.5 \pm 0.2\text{ K}$ .

Our modelling of the supercurrent distributions in these rings is as follows: Consider a thin film ring of thickness  $d$  with radii  $a < b$  in the plane  $z = 0$ . The

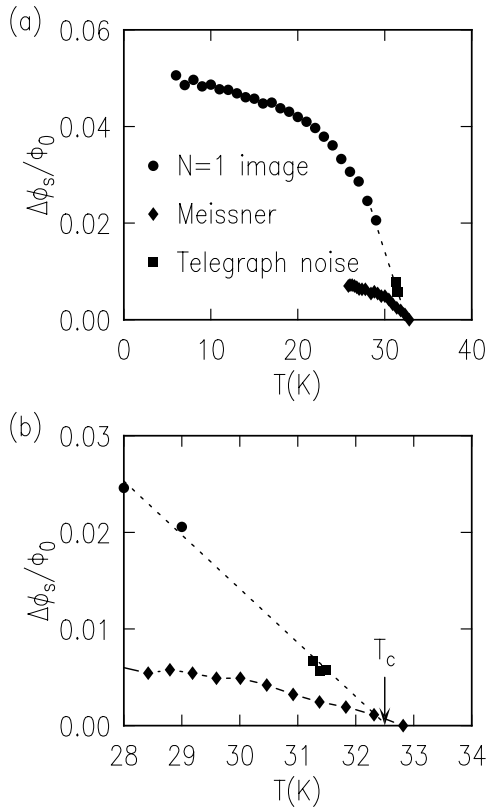


FIG. 2: (a) Difference  $\Delta\phi_s$  in SQUID signal directly above the 80  $\mu\text{m}$  diameter ring minus that with the SQUID far from the ring, with the ring in the  $N = 1$  fluxoid state (solid circles); Meissner screening signal  $\Delta\phi_s$  with an applied induction of 0.2 mG (diamonds); and an amplitude of the telegraph noise due to switching between fluxoid states at  $\phi_a = \phi_0/2$  (squares), all as a function of temperature. (b) Expanded view of the data close to the ring superconducting temperature  $T_c$ .

London equations for the  $\ln$  interior read

$$j = \frac{c_0}{8\pi^2} r + \frac{2}{\phi_0} A; \quad (1)$$

where  $j$  is the supercurrent density,  $\phi_0 = hc/2e$  is the superconducting flux quantum,  $\psi$  is the order parameter phase, and  $A$  is the vector potential. Since the current in the ring must be single valued,  $\psi = N\psi'$ , where  $\psi'$  is the azimuthal angle and the integer  $N$  is the winding number (vorticity) of the state. Integrating  $j$  over the  $\ln$  thickness  $d$ , we obtain:

$$g(r) = \frac{c_0}{4\pi^2} \frac{N}{r} + \frac{2}{\phi_0} A; \quad (2)$$

where  $g(r)$  is the sheet current density directed along the azimuthal  $\psi'$ . The vector potential  $A$  can be written as

$$A(r) = \int_a^z g(\psi) d\psi(r;0) + \frac{r}{2} H; \quad (3)$$

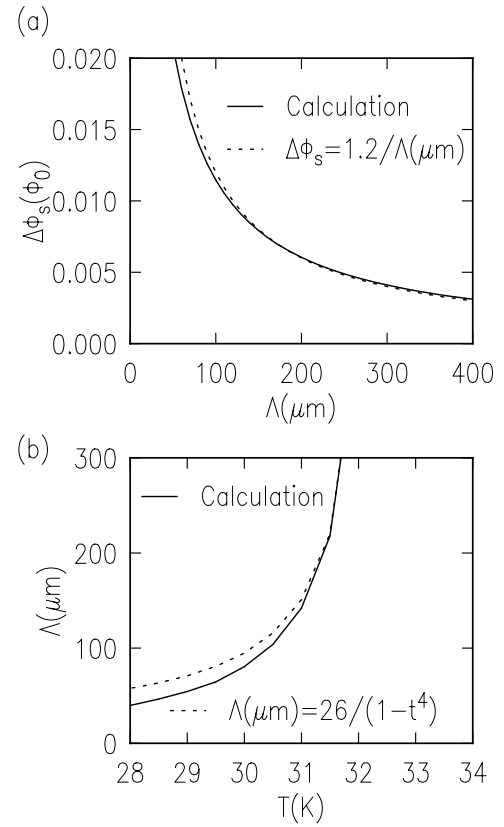


FIG. 3: (a) Calculated dependence of the SQUID difference signal  $\Delta\phi_s$  above minus away from the ring, for the ring and pickup loop geometry used in this paper, as a function of the Pearl length  $\Lambda$  (solid line). The dashed line shows that  $\Delta\phi_s$  is calculated to be nearly inversely proportional to  $\Lambda$ . (b) Calculated dependence of the Pearl length  $\Lambda$  on temperature for the 80  $\mu\text{m}$  ring, assuming the linear dependence of  $\Delta\phi_s$  on temperature indicated by the dashed line in Fig. 2 (solid line). The dashed line is proportional to  $(1 - t^4)^{-1}$ , the ideal temperature dependence for  $\Lambda$ .

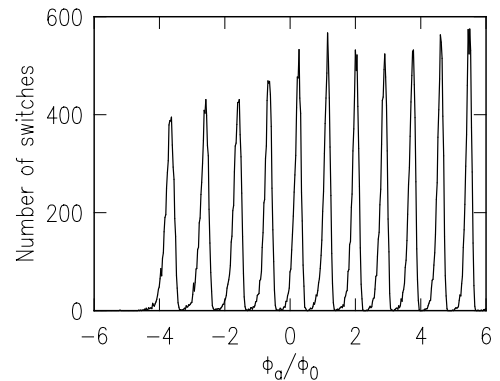


FIG. 4: Histogram of the number of switches observed, as a function of the externally applied flux, for a SQUID pickup loop positioned directly above the 80  $\mu\text{m}$  outer diameter underdeveloped BSCCO ring at  $T = 30.9$  K. The sweep rate was 200  $\phi_0/s$ , with the data stored in 512 bins.

where the last term represents a uniform applied field  $H$  in the  $z$  direction and  $\mathbf{a}(\mathbf{r}; z)$  is the vector potential of the field created by a circular unit current of radius  $a$ :<sup>41</sup>

$$\mathbf{a}(\mathbf{r}; z) = \frac{4}{c} \frac{r-h}{r} \frac{k^2}{2} K(k) \mathbf{e}_i$$

$$k^2 = \frac{4r}{(r+a)^2 + z^2} : \quad (4)$$

Here,  $K(k)$  and  $E(k)$  are the complete elliptic integrals in the notation of Ref. 42.

Substituting Eq. (3) and (4) into (2), we obtain an integrodifferential equation for  $g(r)$ :

$$\frac{4}{c} \frac{d}{dr} (r g(r)) + r^2 H = 0$$

$$= \frac{4}{c} \frac{d}{dr} \left( \frac{h^2 + r^2}{r} K(k_0) \right) + (r+a) E(k_0) \quad (5)$$

where  $k_0^2 = 4r/(r+a)^2$ . This equation is solved by iteration for a given integer  $N$  and field  $H$  to produce current distributions which we label as  $g_N(H; r)$ .

After  $g_N(H; r)$  is found, the field outside the ring can be calculated using Eq. (4):

$$h_z(N; r; z) = \frac{2}{c} \frac{d}{dr} \left( \frac{g_N(H; r)}{r} \right) \frac{h}{r} K(k)$$

$$+ \frac{2}{c} \frac{r^2}{r^2 + z^2} E(k) + H : \quad (6)$$

The flux through the SQUID is obtained numerically by integrating Eq. (6) over the pickup-loop area. The lines in Fig. 1b are two-parameter fits of this integration of Eq. (6) to the data, resulting in  $z = 3.5$  m, and  $a = 7$  m (corresponding to  $r = 1$  m) at  $T = 6$  K, and  $a = 54$  m ( $r = 2.8$  m) at  $T = 30$  K.

This value ( $r = 1$  m) for the low-temperature in-plane penetration depth is at first surprising, given the observed values of  $\lambda_L = 0.2$  m for BSCCO near optimal doping.<sup>43</sup> However, one might expect the penetration depth to be larger for our underdoped films because of their lower  $T_c$ , following the Uemura relation  $\lambda_L \propto T_c^{-2}$ .<sup>44</sup> Further, these films have large normal-state resistivities  $\rho_{ns} \approx 1200$  m $\Omega$ , meaning that they are in the dirty limit, and close to the metal-insulator transition.<sup>45</sup> The zero-temperature penetration depth of a dirty-limit superconductor is given by  $\lambda_L = (\xi/2) \hbar v_F / \mu_0 H_c$ . Taking the BCS value  $\xi = 1.74 k_B T_c$ , with  $T_c = 30$  K gives  $\lambda_L = 0.7$  m. It is expected that fluctuations in the superfluid density could further increase the penetration depth in these layered superconductors.<sup>46</sup>

To model the fluxoid dynamics data presented in this paper, it is necessary to estimate the temperature-dependent Pearl length and the energy associated with supercurrent flow in our rings. We can infer the temperature dependence of the Pearl length from the temperature dependence of  $\lambda_L$  as follows. Numerical integration of Eq. (6) for our ring and SQUID pickup loop geometry

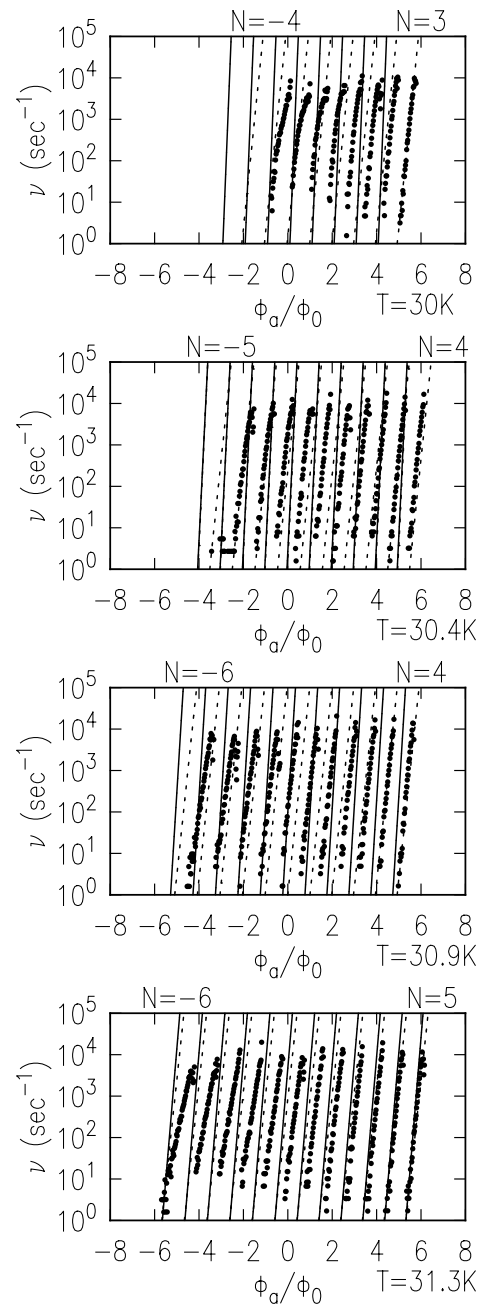


FIG. 5: Fluxoid transition rates for the transition  $N \rightarrow N + 1$  vs. the externally applied flux  $\Phi_a$  (swept towards positive values) for a BSCCO ring of 80  $\mu\text{m}$  outer diameter, with  $T_c = 32.5$  K, at various temperatures. The solid symbols are experimental. The solid and dashed lines are the predictions of the simple model described in the text.

as a function of the Pearl length  $\lambda_P$  gives the solid line in Fig. 3a. The calculated  $\lambda_P$  is nearly inversely proportional to  $\lambda_L$ , as shown by the dashed line in Fig. 3a. The linear dependence of  $\lambda_P$  on temperature indicated by the dashed line in Fig. 2 results in a temperature dependence of the Pearl length  $\lambda_P(T)$  for this ring indicated by the solid line in Fig. 3. Since the London penetration

depth  $l = \frac{p}{1 - t} (t = T/T_c)^{47} = 2^{-2}d$  should be approximately proportional to  $(1 - t)^{-1}$  as indicated by the dashed line in Fig. 3b.

The vorticity number  $N$  of a ring can be changed by varying the externally applied flux  $\Phi_a = H A_{eff}$ , where  $A_{eff}$  is the effective area,<sup>48</sup> and can be monitored by positioning the SQUID pickup loop directly over it.<sup>49</sup> In the limit  $\Phi_a \gg \Phi_0$ , the current around the loop can be found by integrating Eq. (2) to obtain  $A_{eff} = (\Phi_a / \Phi_0) \ln(\Phi_a / \Phi_0)$ . This result also can be obtained from more detailed calculations of  $E(N, H)$ .<sup>50</sup> We assign an experimental value for the effective ring area using the telegraph noise data of Fig. 7, and assuming the peaks are spaced by  $\Phi_0$ . This gives a value of  $2895 \text{ m}^2$ , in comparison with the calculated value of  $2719 \text{ m}^2$ . This discrepancy of about 6% could be due to variations in the photolithography of the rings, or errors in the calibration of the Helmholtz coils which apply the magnetic fields. We used the experimental value for  $A_{eff}$  in determining the flux scales in Figs. 4, 5, and 7. At temperatures sufficiently close to  $T_c$  the vorticity number changes by one vorticity at a time, as determined by the agreement (to within 10%) with our calculations for  $j = 1$  of the measured spacing in applied flux between vortex switching events. Switching distributions  $P(a_{ij})$  were obtained by repeatedly sweeping the applied field, in analogy with measurements of Josephson junctions switching into the voltage state.<sup>51</sup> An example is shown in Fig. 4

The transition rates of the vorticity states were determined from such data using<sup>51</sup>

$$\left( \frac{d a_m}{a} \right) = \frac{d a}{a} \ln \left[ \frac{\sum_{j=1}^8 P(a_{ij})}{\sum_{i=1}^9 P(a_{ji})} \right]; \quad (7)$$

where  $m = 1$  labels the largest  $a$  in a given switching histogram peak, and  $a$  is the flux interval between data points. The dots in Figure 5 show the results from such experiments from the 80  $\mu\text{m}$  ring at several reduced temperatures. The assignment of the starting vorticity number  $N$  in this data was made by following the transitions as they evolved with temperature from the two-state telegraph noise (see Fig. 7) described below.

At temperatures sufficiently close to  $T_c$  and applied fluxes close to a half-integer multiple of  $\Phi_0$ , two-state telegraph noise was observed in the SQUID pickup loop signal when the loop was placed directly above a ring. An example is shown in Fig. 6.

The frequency of this telegraph noise oscillates with the applied flux, with period  $\Phi_0$ , and peaks at  $\Phi_a = (N + 1/2)\Phi_0$ ,  $N$  an integer, as shown in Fig. 7.

### III. DISCUSSION

Several general observations can be made about the vorticity dynamics observed in our experiments. First, the dynamics are nearly periodic in the applied field, with a

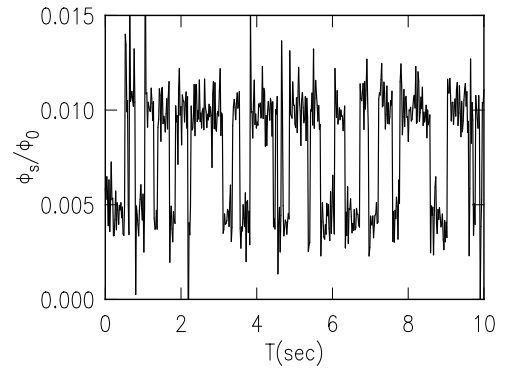


FIG. 6: Telegraph noise signal vs. time for the ring of Figure 4 at  $T = 31.4 \text{ K}$ ,  $a = 0.2$ .

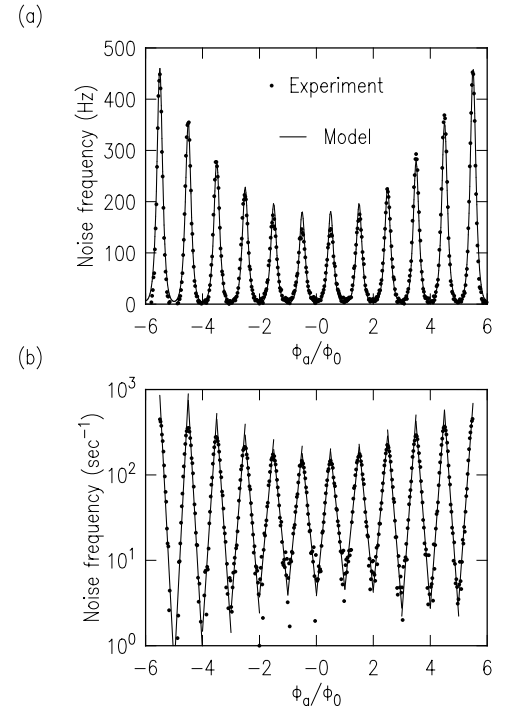


FIG. 7: (a) Telegraph noise signal vs. applied flux  $\Phi_a$  for the 80  $\mu\text{m}$  ring at  $T = 31.6 \text{ K}$ . The dots are the data, the solid line is a fit to the simple model described in the text. (b) Replot of the data of (a) on a log-linear scale. The dots are the data, the solid lines are fits to an exponential dependence on  $a$ , in segments  $N\Phi_0 < a < (N + 1/2)\Phi_0$  and  $(N + 1/2)\Phi_0 < a < (N + 1)\Phi_0$ ,  $N$  an integer.

period given by the applied field times the effective ring area  $A_{eff} = (\Phi_a / \Phi_0) \ln(\Phi_a / \Phi_0)$  (see Figs. 4, 5, and 7). This scaling with the effective ring area has been confirmed for three different ring sizes.

Second, the vorticity transition rates depend exponentially on the applied flux, both for the vorticity escape measurements of Fig. 5, and in the telegraph noise data of Fig. 7. The latter becomes clear when this data is plotted on a log-linear scale, as in Fig. 7(b).

Third, at a particular applied field, both the vorticity

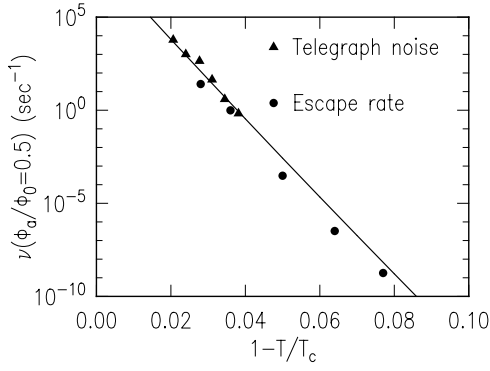


FIG. 8: Plots of the telegraph noise frequency and the vortex transition rate, for the  $N = 0$  to  $N = 1$  transition, at an applied flux of  $\phi_a = \phi_0 = 2$ , as a function of temperature. The symbols are the data; the solid line is a simple model as described in the text. The vortex transition rate data was obtained by extrapolating straight line fits to the data of Fig. 5.

escape rates and the telegraph noise frequencies depend exponentially on temperature. An example for the 80  $\mu\text{m}$  ring is shown in Fig. 8.

We consider the mechanism for transitions between vortex states as a thermally activated nucleation of a vortex in, and transport of this vortex across, the ring wall. The relevant energies in the proposed process are 1) the energy required to nucleate a vortex, and 2) the kinetic and magnetic energies associated with supercurrents in the ring.

The maximum vortex energy in a straight thin superconducting strip of width  $W$  (carrying no transport supercurrent):<sup>52</sup>

$$E_v = \frac{2}{8} \frac{\phi_0^2}{2} \ln \frac{2W}{\xi} : \quad (8)$$

where  $\xi$  is the vortex core size. The energy of the ring in a state with the winding number  $N$  is<sup>53</sup>

$$E_r(N; H) = E_0 (N - \phi_a/\phi_0)^2 : \quad (9)$$

Clearly, the prefactor  $E_0$  coincides with the ring energy in the state  $N = 1$  in zero applied field:

$$E_0 = E_r(1; 0) = \frac{\phi_0^2}{2c} \int_a^b g_{N=1}(0; r) dr ; \quad (10)$$

see Appendix A.

We inferred the temperature dependence of the Pearl length from our SQUID microscope measurements above (see Fig. 3). Once the Pearl length is known, it is possible to calculate the temperature dependence of the energy of our ring. This is done by setting  $N = 1$  and  $H = 0$ , and integrating the solution of Eq. (5) to obtain the total supercurrent, and the total energy in the ring from Eq. (10). Figure 9a shows the results of such a calculation for  $E_0$  as a function of  $\lambda$ . Figure 9b plots  $E_0$  as a function of  $T$  for the 80  $\mu\text{m}$  ring.

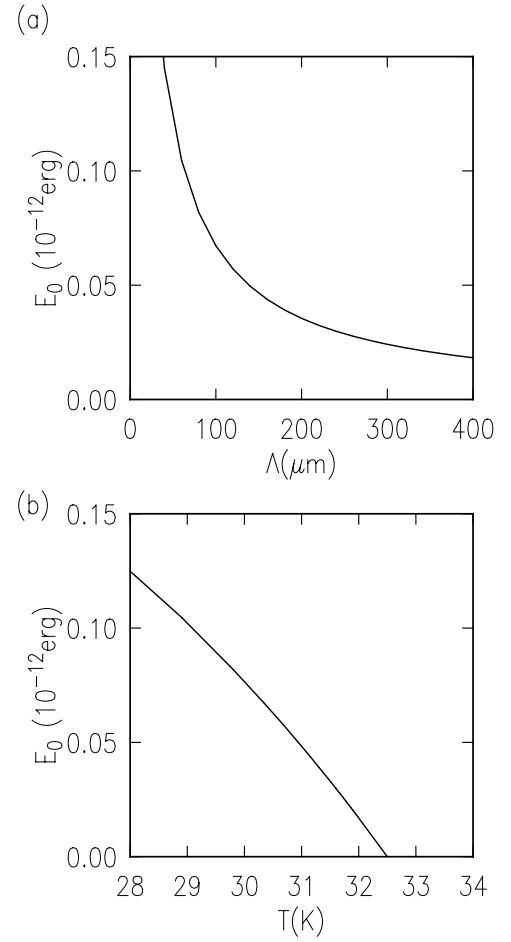


FIG. 9: (a) Calculated dependence of the total energy of our 80  $\mu\text{m}$  outside diameter ring for  $N = 1$ ,  $H = 0$  on the Pearl length  $\lambda$ . (b) Calculated temperature dependence of the total energy for  $N = 1$ ,  $H = 0$ , using the calculated temperature dependence (solid line) of  $\lambda$  from Fig. 3.

Figure 10 shows a simplified schematic of the energies involved in the thermally activated process  $N \rightarrow N + 1$  which is accomplished by a vortex (or an antivortex) crossing the ring. The ring has an initial ring energy  $E_r(N)$ , and a final ring energy  $E_r(N + 1)$ . Within this simple scheme, the energy barrier for the process is

$$\begin{aligned} E &= E_v \left[ H + \frac{E_r(N + 1) + E_r(N)}{2} - E_r(N) \right] \\ &= E_v \left[ H + \frac{E_r(N + 1) - E_r(N)}{2} \right] \\ &= E_v \left[ H + E_0 (N - \phi_a/\phi_0 + 1 = 2) \right]; \quad (11) \end{aligned}$$

Here, we have used Eq. (9); the upper (lower) sign is for a vortex (antivortex) since the corresponding energy is  $\pm H$ .

It should be noted that the simple model we consider here is by no means exact. It disregards an intricate interplay between vortex currents and those flowing in the ring in a certain quantum state  $N$  (the currents in the ring are not a simple superposition of vortex currents

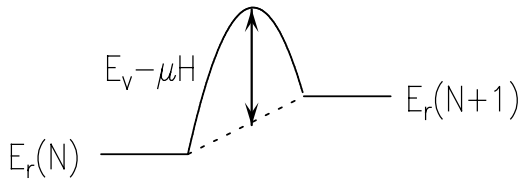


FIG. 10: Schematic energy level diagram for the thermally activated vortex transport mechanism for fluxoid jumps proposed in this paper

and those in the absence of a vortex –even within a linear London approach –because a vortex causes the vorticity  $N$  to depend on the vortex position). For this reason, there is no point –within our model –to calculate “exactly” the magnetic moment; instead, we consider  $\alpha$  as a fitting parameter.

We further simplify the model by considering only transitions between the ground state and the first excited state as in the case of a two-level system. For the two-level system, the RTN rate  $\Gamma = P_1 \nu_1 = P_2 \nu_2$ , where  $P_{1,2}$  are probabilities to find the system in the states 1,2 and  $\nu_{1,2}$  are the lifetimes. Since  $P_1 + P_2 = 1$ , we readily get  $P_{1,2} = \nu_{1,2} / (\nu_1 + \nu_2)$ ,<sup>54</sup> and

$$\Gamma = \frac{1}{\nu_1 + \nu_2} : \quad (12)$$

If the system is in the ground state  $N$ , the closest state of a higher energy depends on the applied field. Using Eq. (9) it is easy to verify that for  $N - 1/2 < \alpha = 0 < N$ , the closest state is  $N - 1$ , whereas for  $N < \alpha = 0 < N + 1/2$ , the first excited state is  $N + 1$ . We begin with the latter possibility. The rate of the transition  $N \rightarrow N + 1$  is

$$\Gamma_{N \rightarrow N+1} = \nu_0 e^{-U_v(N \rightarrow N+1)} + e^{-U_{av}(N \rightarrow N+1)} \quad (13)$$

since the transition can be accomplished by both vortices and antivortices. Here,  $\nu_0$  is an “attempt frequency”,  $U_v$  and  $U_{av}$  denote corresponding barriers divided by  $k_B T$  for vortices and antivortices (for brevity the argument  $\alpha = 0$  of the  $U$ ’s is omitted). This expression can be easily factorized with the help of an identity  $e^x + e^y = 2 \cosh[(x+y)/2] \exp[(x-y)/2]$ :

$$\Gamma_{N \rightarrow N+1} = \frac{\exp[-(U_v + U_{av})/2] \exp[(U_v - U_{av})/2]}{2 \nu_0 \cosh(H/T)} ; \quad (14)$$

where Eq. (11) has been used and for brevity we set  $k_B = 1$ . Similarly we obtain:

$$\Gamma_{N+1 \rightarrow N} = \frac{\exp[-(U_v - U_{av})/2] \exp[(U_v + U_{av})/2]}{2 \nu_0 \cosh(H/T)} : \quad (15)$$

Now Eq. (12) yields

$$\Gamma = \nu_0 e^{-E_v/T} \frac{\cosh(H/T)}{\cosh[E_0(N - \alpha = 0 + 1/2) = T]} : \quad (16)$$

The same calculation for the applied field  $N - 1/2 < \alpha = 0 < N$  gives

$$= \nu_0 e^{-E_v/T} \frac{\cosh(H/T)}{\cosh[E_0(N - \alpha = 0 - 1/2) = T]} : \quad (17)$$

The factors  $1/\cosh[E_0(N - \alpha = 0 - 1/2) = T]$  oscillate with the period  $\alpha = 0 = 1$  because in the ground state the number  $N$  is the closest integer to the value of  $\alpha = 0$ . Due to these factors,  $\Gamma(\alpha = 0)$  has maxima at  $\alpha = 0 = N - 1/2$ . Clearly, the peaks of  $\Gamma(\alpha = 0)$  become sharper when the parameter  $E_0 = T$  increases.

The numerator  $\cosh(H/T)$  provides an increase of the maxima with increasing applied field. Physically, this happens because the vortex magnetic moment reduces the energy barrier by  $H$ . If  $H = T = 1$ , the maxima increase quadratically with field:  $\cosh(H/T) = 1 + H^2/2 = 2T^2$ . This is, in fact, the case for our data. One does not expect  $\Gamma(\alpha = 0)$  to increase without a limit: at a certain applied field, the barrier for the vortex entry splits in two and the vortex can stay in a metastable equilibrium at the ring. Our model does not hold for such fields.

The solid line in Fig. 7 shows a fit of Eqs. (16) and (17) to the experimental data. The best fit parameters were  $\nu_0 = 1.1 \cdot 10^8 \text{ s}^{-1}$ ,  $E_v = 6.03 \cdot 10^{14} \text{ erg}$ ,  $E_0 = 4.98 \cdot 10^{14} \text{ erg}$ , and  $\alpha = 1.93 \cdot 10^{13} \text{ erg/G}$ . From Fig. 3b we read  $(T = 31.6 \text{ K}) = 240 \text{ m}$ . Taking  $\mu = 3.2 \cdot 10^{-27} \text{ J/T}$ ,<sup>55</sup> and  $W = 20 \text{ m}$ , we calculate  $E_v = 1.46 \cdot 10^{13} \text{ erg}$ , a factor of 2.4 larger than the value extracted from the fit. As discussed above, sample inhomogeneities or surface defects<sup>56</sup> could reduce the barrier to entry of vortices in type-II superconductors. From Fig. 9b we read  $E_0 = 2.2 \cdot 10^{14} \text{ erg}$ , smaller than the value obtained from the fit by a factor of 2.3. Our value for the attempt frequency is within the range ( $10^6 - 10^{10} \text{ Hz}$ ) suggested for attempt frequencies from experiments on thermally activated flux jumps in high temperature superconductors.<sup>57,58</sup> Therefore our simple model provides a good description of the magnetic field dependence of the telegraph noise at a fixed temperature, using values for the vortex nucleation energy  $E_v$  and the ring supercurrent energy coefficient  $E_0$  that are within approximately factors of 2 of values calculated from experimental measurements on the same ring.

Note that our estimate of the attempt frequency is very sensitive to the value of the coherence length  $\xi$ . Indeed, the factor  $\exp(-E_v/T)$  combined with  $E_v$  of Eq. (8) yields

$$\Gamma \propto \frac{\nu_0}{2W} \xi^2 = 8^2 T \quad (18)$$

with a large exponent  $\xi^2 = 8^2 T$ .

The same model provides good agreement with the temperature dependence of the fluxoid transition rates and telegraph noise frequencies for the  $N = 0 \rightarrow N = 1$  transition at  $\alpha = 0 = 2$  shown in Fig. 8. The solid line in Fig. 8 is the prediction of Eq. (13), scaling the

value for  $E_v(T)$  at  $T = 31.6$  K from the data of Fig. 7 by  $E_v(T) = E_v(T = 0)(1 - T/T_c)$ .

The solid lines in Fig. 5 show the predictions of Eq. (14), using the simple model outlined above, with the  $T_c$  values from the telegraph noise data of Fig. 7, with  $E_v$  and  $E_0$  scaled in temperature according to the calculated curves in Figs. 3 and 9 respectively. The predictions of the simple model diverge from experiment for lower temperatures and fluxoid numbers. In particular, the simple model predicts that the slope of the fluxoid transition rates with applied flux should increase as the temperature is reduced. However, as can be seen from Fig. 5, although these slopes are relatively insensitive to temperature, if anything they decrease with decreasing temperature. Somewhat better agreement with experiment (the dashed lines in Fig. 5) is obtained if  $E_0$  is taken to have the temperature independent value obtained from the telegraph noise data of Fig. 7, with  $E_v(T) = E_v(T = 0)(1 - T/T_c)$  as before.

We can speculate on some of the sources of the differences between the predictions of our simple model and experiment. First, the simple model does not take into account interactions between the bulk vortex and the supercurrents. As discussed above, we have also implicitly assumed that the rings are spatially homogeneous, with a sharp superconducting transition temperature. The resistive transitions are in fact quite broad. This broadening could be a source of the apparently reduced temperature dependence of  $E_0$  and reduced vortex nucleation energy that we observe. Finally, spatial inhomogeneities could reduce the effective width of the rings.

In summary then, we have measured single fluxoid

transitions and two-state telegraph noise in superconducting thin film rings as a function of applied magnetic field and temperature at temperatures close to  $T_c$ . The long penetration depths in the underdoped cuprate films used allowed measurements over a relatively broad temperature range. The measurements are generally consistent with a model in which the fluxoid transitions are mediated by thermally activated nucleation of a bulk vortex in, and transport of the vortex across, the ring wall. We presented a simple model to explain these results which qualitatively explains some of the features of the data, but other features remain puzzling.

We would like to thank T. Senthil and M. P. A. Fisher for suggesting ring experiments to us, and D. Bonn, W. A. Hardy, R. Koch, K. A. Moler, R. Mints, D. J. Scalapino, F. Tafuri, and S. Woods for useful conversations. This manuscript has been authored in part by Iowa State University of Science and Technology under Contract No. W-7405-ENG-82 with the U.S. Department of Energy. The work of V.G.K. was partially supported by the Binational U.S.-Israel Science Foundation.

#### APPENDIX A

The magnetic part of the energy for the state  $N$  in zero applied field is  $E_m = \int d^2r A \cdot \mathbf{j} = 2c$ . Substitute here the vector potential from Eq. (2) to obtain  $E_m = \int d^2r \left( \frac{1}{2} \mathbf{j}^2 - \frac{1}{2} \mathbf{j} \cdot \nabla \times \mathbf{r} \right) = \int d^2r \left( \frac{1}{2} \mathbf{j}^2 - \frac{1}{2} \mathbf{j} \cdot \nabla \times \mathbf{r} \right)$ . Since the kinetic part is the integral over the volume of the quantity  $\frac{1}{2} \mathbf{j}^2 = \frac{1}{2} \mathbf{j} \cdot \nabla \times \mathbf{r}$ , the first term in  $E_m$  is  $E_{kin}$ . Further,  $\mathbf{j} \cdot \nabla \times \mathbf{r} = N = r$  and we have  $E_m + E_{kin} = \int d^2r (N - 2c)$ .

- 
- <sup>1</sup> B. S. Deaver and W. M. Fairbank, Phys. Rev. Lett. 7, 43 (1961).  
<sup>2</sup> R. Doll and M. Nabauer, Phys. Rev. Lett. 7, 51 (1961).  
<sup>3</sup> G. Aeppli and P. Chandra, Science 275, 177 (1997).  
<sup>4</sup> R. Moessner and S. L. Sondhi, Phys. Rev. B 63, 224401 (2001).  
<sup>5</sup> P. Chandra and B. Douçot, Phys. Rev. B 38, 9335 (1988).  
<sup>6</sup> D. D. Avidovic, S. Kumar, D. H. Reich, J. Siegel, S. B. Field, R. C. Tiberio, R. Hey, and K. P. Bog, Phys. Rev. Lett. 76, 815 (1996).  
<sup>7</sup> D. D. Avidovic, S. Kumar, D. H. Reich, J. Siegel, S. B. Field, R. C. Tiberio, R. Hey, and K. P. Bog, Phys. Rev. B 55, 6518 (1997).  
<sup>8</sup> V. B. Geshkenbein and A. I. Larkin, JETP Lett. 43, 395 (1986).  
<sup>9</sup> V. B. Geshkenbein, A. I. Larkin and A. Barone, Phys. Rev. B 36, 235 (1987).  
<sup>10</sup> M. Sigrist and T. M. Rice, J. Phys. Soc. Japan 61, 4283 (1992).  
<sup>11</sup> D. J. Van Harlingen, Rev. Mod. Phys. 67, 515 (1995).  
<sup>12</sup> C. C. Tsuei and J. R. Kirtley, Rev. Mod. Phys. 72, 969 (2000).  
<sup>13</sup> L. N. Bulaevski, V. V. Kuzii, and A. A. Sobyani, JETP Lett. 25, 290 (1977).  
<sup>14</sup> V. V. Ryazanov, V. A. Oboznov, A. Y. Rusanov, A. V. Veretennikov, A. A. Golubov, and J. Aarts, Phys. Rev. Lett. 86, 2427 (2001).  
<sup>15</sup> V. V. Ryazanov, V. A. Oboznov, A. V. Veretennikov, and A. Y. Rusanov, Phys. Rev. B 65, 020501 (2002).  
<sup>16</sup> H. J. H. Smilde, H. Hilgenkamp, G. Rijnders, H. Rogalla and D. H. A. Blank, Appl. Phys. Lett. 80, 4579 (2002).  
<sup>17</sup> H. J. H. Smilde, A. Riando, D. H. A. Blank, G. J. G. Erritsan, H. Hilgenkamp and H. Rogalla, Phys. Rev. Lett. 88, 057004 (2002).  
<sup>18</sup> H. Hilgenkamp, A. Riando, H.-J. Smilde, D. H. A. Blank, G. Rijnders, H. Rogalla, J. R. Kirtley, and C. C. Tsuei, to be published in Nature.  
<sup>19</sup> T. Senthil and M. P. A. Fisher, Phys. Rev. Lett. 86, 292 (2001).  
<sup>20</sup> D. A. Bonn, J. C. Wynn, B. W. Gardner, Ju Lin Yu, R. Liang, W. N. Hardy, J. R. Kirtley, and K. A. Moler, Nature 414, 887 (2001).  
<sup>21</sup> J. C. Wynn, D. A. Bonn, B. W. Gardner, Yu-Ju Lin, Ruixing Liang, W. N. Hardy, J. R. Kirtley, and K. A. Moler, Phys. Rev. Lett. 87, 197002 (2001).  
<sup>22</sup> T. W. B. Kibble, J. Phys. A 9, 1387 (1976).  
<sup>23</sup> T. W. B. Kibble, Phys. Rep. 67, 183 (1980).  
<sup>24</sup> W. H. Zurek, Physics Reports 276, 177 (1996).  
<sup>25</sup> R. Carmi and E. Polturak, Phys. Rev. B 60, 7595 (1999).  
<sup>26</sup> R. Carmi, E. Polturak, and G. Koren, Phys. Rev. Lett. 84,

- 4966 (2000).
- <sup>27</sup> E. Kavoussanaki, R. Monaco, and R. J. Rivers, *Phys. Rev. Lett.* 85, 3452 (2000).
- <sup>28</sup> M. Ghinovker, B. Ya. Shapiro, and I. Shapiro, *Europhys. Lett.* 53, 240 (2001).
- <sup>29</sup> J. E. Mooij et al., *Science* 285, 1036 (1999).
- <sup>30</sup> C. Van der Wal, et al., *Science* 290, 773 (2000).
- <sup>31</sup> J. R. Friedman, V. Patel, W. Chen, S. K. Tolpygo, and J. E. Lukens, *Nature* 406, 43 (2000).
- <sup>32</sup> G. B. Latter, M. V. Feigel'man, V. B. Geshkenbein, A. I. Larkin, and V. M. Vinukur, *Rev. Mod. Phys.* 66, 1125 (1994).
- <sup>33</sup> I. L. Landau and H. R. Ott, *Phys. Rev. B* 63, 184516 (2001).
- <sup>34</sup> M. J. Ferrari, M. Johnson, F. C. Wellstood, J. J. Kingston, T. J. Shaw, and J. Clarke, *J. Low. Temp. Phys.* 94, 15 (1994).
- <sup>35</sup> see, for example R. Rouse, Siyuan Han, and J. E. Lukens, *Phys. Rev. Lett.* 75, 1614 (1995), and references therein.
- <sup>36</sup> X. Zhang and J. C. Price, *Phys. Rev. B* 55, 3128 (1997).
- <sup>37</sup> J. Pearl, *J. Appl. Phys.* 37, 4139 (1966).
- <sup>38</sup> T. Watanabe, T. Fujii, and A. Matsuda, *Phys. Rev. Lett.* 79, 2113 (1997).
- <sup>39</sup> Z. Konstantinovic, Z. Z. Li, and H. Ray, *Physica B* 259–261, 567 (1999).
- <sup>40</sup> J. R. Kirtley, M. B. Ketchen, K. G. Stawiasz, J. Z. Sun, W. J. Gallagher, S. H. Banton, and S. J. Wind, *Appl. Phys. Lett.* 74, 4011 (1999).
- <sup>41</sup> L. D. Landau and E. M. Lifshitz, *Electrodynamics of Continuous Media*, Pergamon, NY, 1984.
- <sup>42</sup> I. S. Gradshteyn and I. M. Ryzhik, *Tables of Integrals*, Academic Press, NY, 1980.
- <sup>43</sup> O. Waldmann, F. Steinmeyer, P. Müller, J. J. Neumeier, F. X. Regi, H. Savary, and J. Schneck, *Phys. Rev. B* 53, 11825 (1996).
- <sup>44</sup> Y. J. Uemura et al. *Phys. Rev. Lett.* 62, 2317 (1989).
- <sup>45</sup> K. Semba and A. Matsuda, *Phys. Rev. Lett.* 86, 496 (2001).
- <sup>46</sup> S. N. Artemenko and S. V. Remizov, *Phys. Rev. Lett.* 86, 708 (2001).
- <sup>47</sup> M. Tinkham, *Introduction to Superconductivity*, McGraw-Hill, New York, 1975, p. 80.
- <sup>48</sup> M. B. Ketchen, W. J. Gallagher, A. W. Kleinsasser, S. Murphy, and J. R. Clem, *SQUID '85: Superconducting Quantum Interference Devices and Their Applications*, ed. H. D. Hahlbohm and H. Lubbig, Walter de Gruyter, Berlin, 1985, p. 865.
- <sup>49</sup> C. C. Tsuei, J. R. Kirtley, C. C. Chi, Lock See Yu-Jahnes, A. Gupta, T. Shaw, J. Z. Sun, and M. B. Ketchen, *Phys. Rev. Lett.* 73, 593 (1994).
- <sup>50</sup> V. Kogan, J. Clem, R. Mints, and J. R. Kirtley, unpublished.
- <sup>51</sup> T. A. Fulton and L. N. Dunkelberger, *Phys. Rev. B* 9, 4760 (1974).
- <sup>52</sup> V. G. Kogan, *Phys. Rev. B* 49, 15874 (1994). Although this paper has an error, the results are correct for sample sizes small relative to the Pearl length.
- <sup>53</sup> A. Barone and G. Paterno, *Physics and Applications of the Josephson Effect*, Wiley, New York, 1982, p. 355.
- <sup>54</sup> S. Machlup, *J. Appl. Phys.* 25, 341 (1954).
- <sup>55</sup> P. Seidell, M. G. Rajar, A. P. Lecenik, and R. H. Ubina, *Physica B* 218, 229 (1996).
- <sup>56</sup> D. Yu. Vodolazov, I. L. Maksimov, and E. H. Brandt, cond-mat/0101074 (2001).
- <sup>57</sup> A. C. Risan, P. Badica, S. Fujiwara, J. C. Nie, A. Sundaresan, Y. Tanaka, and H. Thara, *Appl. Phys. Lett.* 80, 3556 (2002).
- <sup>58</sup> Y. Yeshurun, A. P. Malozemov, and A. Shaulov, *Rev. Mod. Phys.* 68, 911 (1996).